Wide-angle infrared absorber based on a negative-index plasmonic metamaterial

Yoav Avitzour,[1] Yaroslav A. Urzhumov,[2] and Gennady Shvets[1]
[1]*Department of Physics, The University of Texas at Austin, Austin, Texas 78712, USA*
[2]*COMSOL, Inc., 10850 Wilshire Boulevard 800, Los Angeles, California 90024, USA*
(Received 5 December 2008; published 30 January 2009)

A metamaterial-based approach in making a wide-angle absorber of infrared radiation is described. The technique is based on an anisotropic perfectly impedance-matched negative-index material (PIMNIM). It is shown analytically that a PIMNIM that is subwavelength in all three dimensions enables absorption close to 100% for incidence angles up to 45° to the normal. A specific implementation of such frequency-tunable PIMNIM based on plasmonic metamaterials is presented. Applications to infrared imaging and coherent thermal sources are described.

DOI: 10.1103/PhysRevB.79.045131 PACS number(s): 78.20.Ci, 42.25.Bs, 42.70.−a, 78.20.Bh

I. INTRODUCTION

The emergence of a new field of electromagnetic metamaterials was brought about by the demand for materials with exotic properties unattainable in nature. One such property is a negative refractive index that requires both the effective dielectric permittivity ϵ_{eff} and magnetic permeability μ_{eff} to be negative.[1,2] Applications of negative-index metamaterials (NIMs) include "perfect" lenses, subwavelength transmission lines and resonators, and miniature antennas among others.[3–5]

The results reported in this paper pertain to two other recently emerged applications of metamaterials. The first one is wavelength-selective infrared[6] and terahertz[7,8] detection, which is important for thermal imaging, night vision, and nondestructive detection. Wide-angle power absorption efficiency is desirable for miniaturizing photodetectors or microbolometers down to the wavelength size. The second application is the development of coherent thermal emitters[9–12] for spectroscopic and thermophotovoltaic (TPV) (Refs. 13 and 14) applications. By virtue of Kirchhoff's law, emissivity of a thermal emitter approaches the blackbody limit only if the absorptivity approaches unity. Moreover, wavelength-selective radiators can dramatically improve the efficiency of current generation in a TPV cell[13,14] if their emission spectrum is matched to the bandgap of the TPV converter. For example, a typical TPV converter, GaSb, has the bandgap of $E_G=0.7$ eV that would be ideally suited to a wavelength-selective radiator operating in near infrared (around $\lambda=1.7$ μm). For spectroscopic applications, arrays of wavelength-sized narrow-band coherent thermal emitters based on a metamaterial unit cell can be designed. The emitted radiation of each detector is focusable to wavelength-sized spots using large numerical aperture optics. With these applications in mind, we describe in this paper an ultrathin metamaterial-based wide-angle absorber of near-infrared radiation. The design of this perfect absorber is inspired by a perfectly impedance-matched negative-index metamaterial (PIMNIM) constructed from plasmonic wires.

II. THEORETICAL BACKGROUND

As a background, we consider a simple problem of radiation absorption by a semi-infinite slab of a lossy metamaterial with engineered dielectric permittivity and magnetic permeability tensors $\bar{\bar{\epsilon}}$ and $\bar{\bar{\mu}}$. Radiation is assumed to be incident in the x-z plane at an angle θ with respect to the vacuum-material interface normal $\vec{e}_x$. We further assume s polarization of the incident wave as shown in the inset of Fig. 1, i.e., the only nonvanishing field components are E_y, H_x, and H_z. Assuming that both $\bar{\bar{\epsilon}}$ and $\bar{\bar{\mu}}$ are diagonal tensors, their only relevant components are ϵ_{yy}, μ_{xx}, and μ_{zz}. For our semi-infinite slab (assuming that the metamaterial thickness L_x is sufficient to absorb all transmitted radiation), absorptivity A is limited only by reflection. A straightforward calculation yields the reflection r and absorption $A=1-|r|^2$ coefficients,

$$A = 1 - \left| \frac{\cos\theta - \sqrt{\epsilon_{yy}/\mu_{zz} - \sin^2\theta/(\mu_{zz}\mu_{xx})}}{\cos\theta + \sqrt{\epsilon_{yy}/\mu_{zz} - \sin^2\theta/(\mu_{zz}\mu_{xx})}} \right|^2, \qquad (1)$$

where all material parameters are, in general, wavelength dependent.

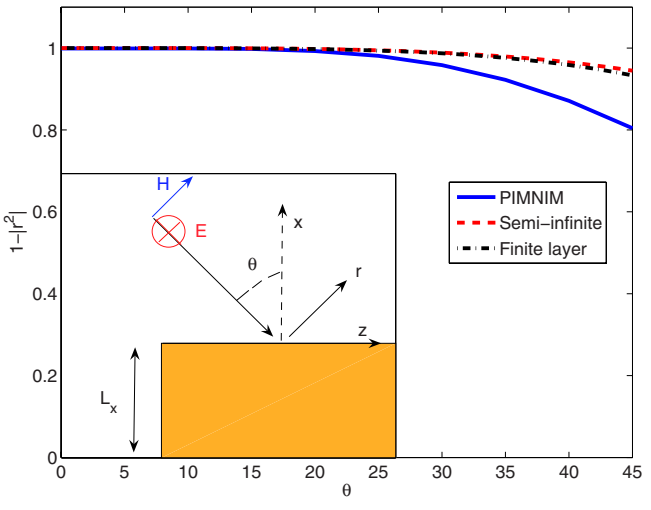

FIG. 1. (Color online) Angular dependence of the absorption coefficient for the idealized structure with $\mu_{zz}=\epsilon_{yy}=-1+i$, $\mu_{xx}=1$, $L_x=\infty$ (dashed line), and $L_x=200$ nm (dashed-dotted line), barely distinguishable from the $L_x=\infty$ line. Solid line: same for the specific implementation of the metamaterial absorber shown in Fig. 2. A schematic of the idealized wide-angle metamaterial absorber is given in the inset; s-polarized incident wave is assumed.

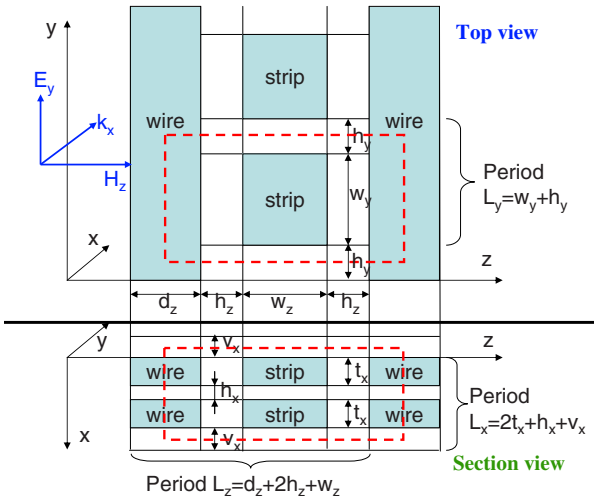

FIG. 2. (Color online) Schematic of the PIMNIM structure. Unit cell for electromagnetic and electrostatic simulations is inside the dashed rectangles.

Studying Eq. (1), we note that total absorption $[A(\lambda_0)\equiv 1]$ at a specific wavelength λ_0 is achievable at normal incidence ($\theta=0$) if the absorber material impedance $\eta=\sqrt{\mu_{zz}/\epsilon_{yy}}$ is matched to that of vacuum, i.e., when $\mu_{zz}(\lambda_0)=\epsilon_{yy}(\lambda_0)$. Using impedance matching to achieve total absorption is a very well-known approach in microwave engineering.[15,16] More surprising is another prediction of Eq. (1) that nearly total absorption can be achieved over a very broad range of angles. Assuming that $\mu_{xx}(\lambda_0)=1$ and $|\mu_{zz}|=|\epsilon_{yy}|\gg 1$, we find that $A(\lambda_0)\approx 1-\tan^4\theta/2$. For a 90° full angle ($\theta_{\max}=\pi/4$) we find that $0.97<A<1$ for $0<\theta<\theta_{\max}$. Even more remarkably, a similarly high broad-angle absorption is predicted even for much more modest values of μ_{zz} and ϵ_{yy}. For example, if the absorbing medium is a NIM (Refs. 1 and 2) with $\epsilon_{yy}=\mu_{zz}=-1+i$, we find that $0.94<A<1$. The angular dependence $A(\theta)$ for such PIMNIM is shown in Fig. 1 for the semi-infinite metamaterial slab, $L_x=\infty$, as well as for the more general case of a finite slab with $L_x\approx\lambda_0/7$. The two curves are barely distinguishable because of the high metamaterial loss.

The main implication of these results is that a subwavelength slab of *almost any* impedance-matched metamaterial acts as a wide-angle absorber. The challenge now is to design such a metamaterial, especially in the technologically important infrared part of the spectrum. With this goal in mind, the rest of this paper is organized as follows. In Sec. III we present one such possible metamaterial design based on two layers of alternating long and short plasmonic nanoantennas (Fig. 2) and demonstrate that the unit cell of this PIMNIM can be made highly subwavelength in near infrared. The subwavelength requirement is critical for achieving wide-angle absorption; recent numerical simulations[16] have found that $A(\theta)$ rapidly drops with θ when the unit cell is too large. Then, in Sec. IV, we demonstrate that a single layer of PIMNIM enables optical absorption $0.7<A(\theta)<0.9$ for a 90° full-angle scan and that its small-angle absorption coefficient exactly agrees with the prediction of Eq. (1). Finally, in Sec. V we show that extremely high optical intensity enhancements (at least $\times 10^3$) can be produced at the absorption peak.

III. PIMNIM DESIGN

The geometry of the unit cell of the proposed PIMNIM is shown in Fig. 2. Each unit cell consists of two parallel layers separated by the distance h_x. Each layer consists of a cut wire of width w_z and length w_y surrounded by the continuous in the y-direction wires of width d_z. To enable planar fabrication, the heights t_x of the cut and continuous wires are assumed to be the same. Metal wires are assumed to be embedded inside a dielectric with $\epsilon_d=2.25$. An s-polarized electromagnetic wave $\vec{E}\|\vec{e}_y$ excites the electric and magnetic responses of the unit cell. The magnetic response is caused by counterpropagating currents flowing through the adjacent cut wires. Both cut and continuous wires contribute to the electric response. A similar structure has been analyzed in the microwave part of the spectrum,[17] where it is not subwavelength. *Plasmonic effects*, i.e., taking into account that metals have a finite dielectric permittivity $\epsilon_m\equiv\epsilon_m'+i\epsilon_m''$ with $\epsilon_m'<0$, are *necessary* to miniaturize the unit cell.

Electromagnetic resonances in effective permittivity ϵ_{eff} and magnetic permeability μ_{eff} of plasmonic composites are unambiguously related[18–20] to the electrostatic surface-plasmon resonances of the appropriate symmetry (electric dipole and magnetic dipole, correspondingly). Therefore, the first step in investigating the suitability of a particular unit-cell geometry for a plasmonic NIM is to identify the frequencies of its electrostatic resonances. Specifically, magnetic activity (including negative-index behavior) has been shown to exist[18] only for $\lambda>\lambda_{\text{es}}$, where $\lambda_{\text{es}}\equiv 2\pi c/\omega_{\text{es}}$ is the vacuum wavelength corresponding to the frequency of the electrostatic resonance responsible for the magnetic activity. Such magnetically active (MA) resonance of the PIMNIM structure has been calculated by solving the Poisson equation $\vec{\nabla}\cdot(\epsilon\vec{\nabla}\phi)=0$ for the electrostatic potential ϕ, where ϵ is a piecewise constant function equal to ϵ_m inside the metal wires and ϵ_d outside. Poisson's equation can be solved as a generalized eigenvalue equation[20–22] to yield the values of ϵ_m corresponding to the electrostatic resonances.

Potential distribution of the lowest-frequency MA resonance is shown in Fig. 3. Its magnetic nature can be deduced from the electric field loops formed between the two cut wires. The above resonance occurs when the dielectric contrast between metal wires and the dielectric matrix is $\epsilon_m/\epsilon_d=-26.8$. Because the resonant dielectric contrast is determined from electrostatic calculations that contain no spatial scale, this value is determined by the *geometric shape* of the unit cell and its inclusions but not by the overall scale set by either of the periods $L_{x,y,z}$. Assuming gold as the plasmonic component and silica with $\epsilon_d=2.25$ as an embedding dielectric, the electrostatic resonance occurs at $\lambda_{\text{es}}=1.2$ μm, thereby setting the lower limit on the wavelength at which strong magnetic response is expected. The next, electrically active (EA) resonance corresponds to $\epsilon_m/\epsilon_d=-19$, is considerably blueshifted from the MA resonance. Therefore, the PIMNIM structure depicted in Fig. 3 is promising as a NIM that has widely separated electric and magnetic resonances. Thus, its electromagnetic characteristics strongly resemble those of the original microwave NIMs.[2] The important difference is that the proposed structure operates at the near-

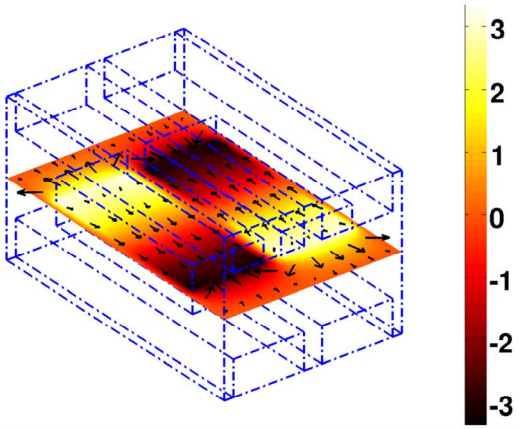

FIG. 3. (Color online) Electrostatic magnetically active plasmon resonance of the PIMNIM structure shown in Fig. 2 with the scalable geometric proportions corresponding to (in nm) L_y=320, w_y=200, t_x=80, w_z=50, d_z=80, h_x=20, v_x=10, and h_z=20. The resonance occurs at ϵ_m/ϵ_d=−26.8. Arrows: electric field; color: electrostatic potential.

infrared frequencies and exploits plasmonic resonances to achieve sub-λ_d cell size, where λ_d is the wavelength inside the substrate.

It is instructive to compare the resonant frequency of the MA resonance of the PIMNIM structure with that of the traditional double-fishnet (DF) (Refs. 23 and 24) structure. DF can be obtained from the PIMNIM by extending the cut wires in z direction until they merge with continuous wires running along the y axis, thereby forming the second orthogonal set of continuous wires in the z direction. For example, the DF structure thus obtained from the PIMNIM structure shown in Fig. 3 is periodic in the y-z plane with the periods of L_z=170 nm and L_y=320 nm, containing two sets of intersecting metal strips in the y and z directions, with the corresponding widths of d_z=80 nm and w_y=200 nm. The MA plasmonic resonance is found at ϵ_m/ϵ_d=−8.3 which corresponds to λ_{es}=0.73 μm for gold. Of course, the physical sizes can be scaled from the above dimensions by an arbitrary factor because there is no physical scale in electrostatics. This simulation illustrates the challenge of making a strongly sub-λ_d DF structure. For the unit cell to be sub-λ_d, the operational wavelength must be reasonably close to λ_{es}. Therefore, making a unit cell with the largest dimension of $\lambda/4$ requires L_y<200 nm. Such small DF structures have never been fabricated to date, which explains why sub-λ_d DF-based NIMs have never been produced.

IV. SIMULATION RESULTS

Full electromagnetic finite element frequency domain (FEFD) simulations of light transmission/reflection through the PIMNIM structure shown in Fig. 2 (approximate physical parameters indicated in Fig. 3 and further optimized to achieve perfect impedance matching) were carried out using the COMSOL (Ref. 25) commercial package. Drude model for $\epsilon_m(\omega)$ of gold, with ω_p=1.367×10^{16} rad/s and γ=4×10^{13} rad/s (taken from Ref. 26), and substrate permittivity

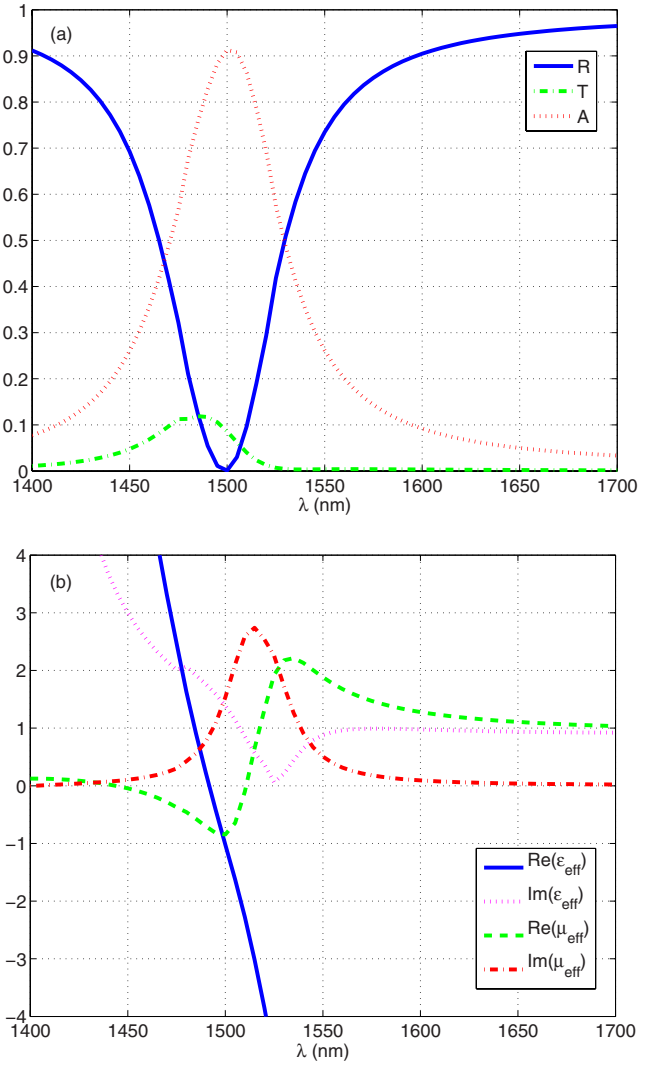

FIG. 4. (Color online) (a) Reflectance, transmittance, and absorbance at normal incidence of a single PIMNIM layer. (b) Extracted effective dielectric permittivity ϵ_{eff} and magnetic permeability μ_{eff} of the PIMNIM structure. Reflectance vanishes at λ=1.5 μm because $\epsilon_{\text{eff}}=\mu_{\text{eff}}$. Parameters (in nm): L_y=326, w_y=208, t_x=80, w_z=46, d_z=78, h_x=21, and h_z=20.

ϵ_d=2.25 were used in the simulations. Reflection minimization was carried out using standard nonlinear multivariable optimization to fine tune the PIMNIM parameters and adjust the perfect-matching wavelength λ_0. The normal incidence (θ=0) results are shown in Fig. 4(a); zero reflection is achieved (by design) at λ_0=1.5 μm, with the single PIMNIM layer absorption coefficient $A\approx 0.9$ (or $A\approx 0.99$ for two layers).

Effective parameters $\epsilon_{yy}\equiv\epsilon_{\text{eff}}(\lambda)$ and $\mu_{zz}\equiv\mu_{\text{eff}}(\lambda)$ of the PIMNIM structure were extracted from the complex transmission and reflection coefficients through a single PIMNIM layer using the standard procedure.[27] Because the negative-index band is the lowest (in frequency) transmission band of the PIMNIM, there is no ambiguity in determining ϵ_{eff} and μ_{eff}. At the impedance matching point λ_0=1.5 μm it is found that $\epsilon_{\text{eff}}=\mu_{\text{eff}}=-0.85+1.4i$. Although the so-called figure of merit (FOM=Re n/Im n) is less than unity, achieving

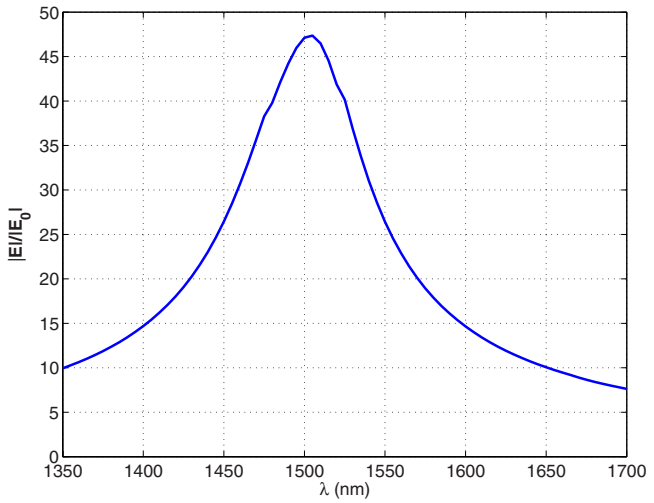

FIG. 5. (Color online) Maximum field enhancement, $|\boldsymbol{E}|/|E_0|$, in the PIMNIM vs wavelength. It is noted that the enhancement is maximized at the absorption peak and has no features corresponding to the electric resonance at $\lambda = 1380$ nm.

high FOM is not necessary (or even desirable) for accomplishing total wide-angle absorption. More important is ensuring that the unit cell of the PIMNIM is very subwavelength: $L_{x,y,z} \ll \lambda_d$. This is indeed accomplished by the present PIMNIM design: $n_d L_y/\lambda_0 \approx 0.3$.

The peak absorption, $A_{\max}(\theta) \equiv 1 - |r|^2(\theta)$, of the PIMNIM is plotted in Fig. 1. For small θ there is an excellent agreement between $A_{\max}$ and Eq. (1), indicating that the PIMNIM is accurately described as an effective medium. Even for $\theta = \pm 45°$ absorptivity remains at about 70%. This implies that in a narrow spectral interval around λ_0, emissivity of a heated PIMNIM is close to that of a blackbody over a broad range of angles, which would enable to manufacture wavelength-sized coherent thermal emitters.

V. FIELD ENHANCEMENT

Physically, the absorption peak corresponds to strong electric field enhancement inside the PIMNIM structure. For example, for the PIMNIM described by Fig. 4, it is found that the maximum intensity enhancement near the corners and edges of the cut wire exceeds $|E_{\max}|^2/|E_0|^2 > 2000$, where E_0 is the amplitude of the incident wave, as can be seen in Fig. 5. We note that calculating the maximum field in the simulation domain can be imprecise because mesh irregularities can lead to mesh-dependent spikes at the corners and edges of the structure. In order to calculate the field enhancement while avoiding such numerical artifacts, the results presented in Fig. 5 were calculated by taking the maximum of $|\boldsymbol{E}|$ interpolated on a rectangular grid of $1 \times 1 \times 1$ nm^3 and then smoothed by nearest-neighbor smoothing. This method was found to be robust under variations in mesh structure and density. Interestingly, the field enhancement is maximized at the absorption peak, at $\lambda = 1.5$ μm, yet shows no structure near the electric resonance, at $\lambda = 1.38$ μm. This can be explained by the very strong reflection at the electric resonance, which prevents the incident fields from penetrating into structure.

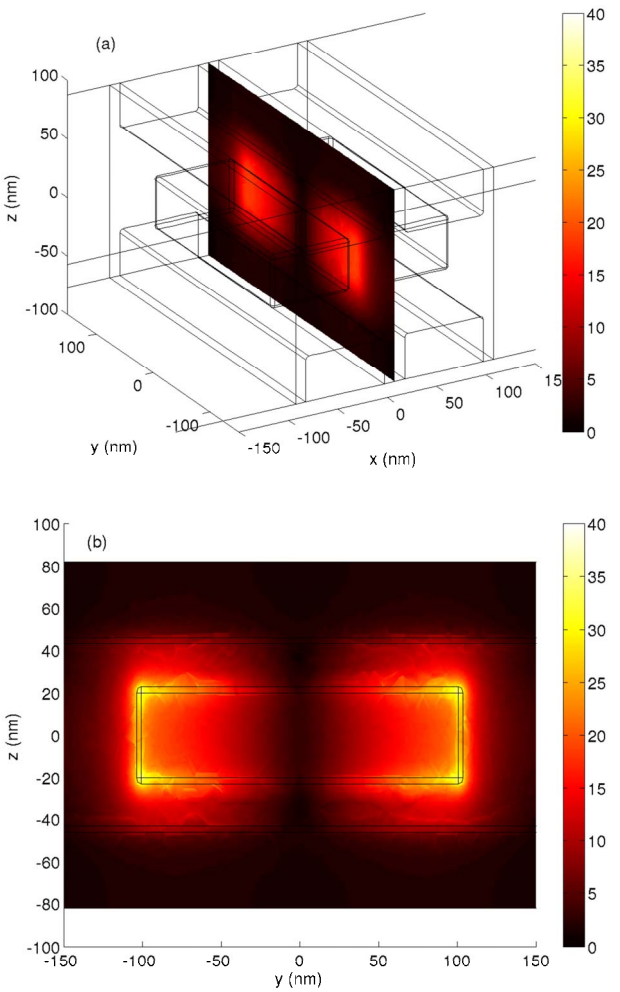

FIG. 6. (Color online) Field enhancement, $|\boldsymbol{E}|/|E_0|$, in the PIMNIM. Field is plotted on y-z slices at (a) $x=0$ and (b) $x=-8$ nm. Although the largest enhancement is near the edges and corners, a relatively large area experiences significant enhancement.

In addition to the enhancement near the corners and edges of the structure, fairly large field enhancement exists in a considerable volume between the cut wires. Figure 6 presents $|\boldsymbol{E}|$ at two y-z cross sections for different values of x. In Fig. 6(a) the magnitude of the electric field $|\boldsymbol{E}|$ is plotted at $x=0$ (in the middle of the PIMNIM). Intensity enhancement of $|\boldsymbol{E}|^2/|E_0|^2 \approx 200$ is apparent in about two thirds of the region between the front and the back cut wires. Figure 6(b) presents the field closer the front cut wire at $x=-8$ nm. An average intensity enhancement of $|\boldsymbol{E}|^2/|E_0|^2 \approx 400$ is apparent in roughly the same area. If photon-counting detectors are integrated into the PIMNIM structure, then such intensity enhancement translates into proportionally enhanced absorption efficiency. The consequence of the large field enhancement is the desirable ultrathin dimension of the absorber, in contrast to earlier calculations[28] that demonstrated that thicker (about one wavelength) perfect absorbers can be developed using plasmonic spheres.

VI. CONCLUSIONS

In conclusion, we have demonstrated that an impedance-matched negative-index metamaterial can act as a

wavelength-selective wide-angle absorber of infrared radiation. A specific implementation of such frequency-tunable PIMNIM based on plasmonic metamaterials is presented. Applications of the PIMNIM include infrared imaging and coherent thermal sources.

ACKNOWLEDGMENTS

This work was supported by the AFOSR MURI under Grants No. FA9550-06-1-0279 and No. FA9550-08-1-0394, and the NSF NIRT under Grant No. 0709323.

[1] V. G. Veselago, Sov. Phys. Usp. **10**, 509 (1968).
[2] D. R. Smith, W. J. Padilla, D. C. Vier, S. C. Nemat-Nasser, and S. Schultz, Phys. Rev. Lett. **84**, 4184 (2000).
[3] J. B. Pendry, Phys. Rev. Lett. **85**, 3966 (2000).
[4] A. Alu and N. Engheta, IEEE Trans. Microwave Theory Tech. **52**, 199 (2004).
[5] A. Alu, N. Engheta, A. Erentok, and R. W. Ziolkowski, IEEE Antennas Propag. Mag. **49**, 23 (2007).
[6] S.-W. Han, J.-W. Kim, Y.-S. Sohn, and D. P. Neikirk, Electron. Lett. **40**, 1410 (2004).
[7] H. Tao, N. I. Landy, S. M. Bingham, X. Zhang, R. D. Averitt, and W. J. Padilla, Opt. Express **16**, 7181 (2008a).
[8] H. Tao, C. M. Bingham, A. C. Strikwerda, D. Pilon, D. Shrekenhamer, N. I. Landy, K. Fan, X. Zhang, W. J. Padilla, and R. D. Averitt, Phys. Rev. B **78**, 241103(R) (2008).
[9] J. G. Fleming, S. Y. Lin, I. El-Kady, R. Biswas, and K. M. Ho, Nature (London) **417**, 52 (2002).
[10] D. L. C. Chan, M. Soljačić, and J. D. Joannopoulos, Phys. Rev. E **74**, 036615 (2006).
[11] J.-J. Greffet, R. Carminati, K. Joulain, J.-P. Mulet, S. Mainguy, and Y. Chen, Nature (London) **416**, 61 (2002).
[12] S. Ingvarsson, L. J. Klein, Y.-Y. Au, J. A. Lacey, and H. F. Hamann, Opt. Express **15**, 11249 (2007).
[13] T. J. Coutts, Renewable Sustainable Energy Rev. **3**, 77 (1999).
[14] M. Laroche, R. Carminati, and J.-J. Greffet, J. Appl. Phys. **100**, 063704 (2006).
[15] J. Y. Shin and J. H. Oh, IEEE Trans. Magn. **29**, 3437 (1993).
[16] N. I. Landy, S. Sajuyigbe, J. J. Mock, D. R. Smith, and W. J. Padilla, Phys. Rev. Lett. **100**, 207402 (2008).
[17] M. Kafesaki, I. Tsiapa, N. Katsarakis, T. Koschny, C. M. Soukoulis, and E. N. Economou, Phys. Rev. B **75**, 235114 (2007).
[18] Y. Urzhumov and G. Shvets, Solid State Commun. **146**, 208 (2008).
[19] Y. Urzhumov, G. Shvets, J. Fan, F. Capasso, D. Brandl, and P. Nordlander, Opt. Express **15**, 14129 (2007).
[20] G. Shvets and Y. A. Urzhumov, Phys. Rev. Lett. **93**, 243902 (2004).
[21] D. J. Bergman and D. Stroud, Solid State Phys. **46**, 147 (1992).
[22] M. I. Stockman, S. V. Faleev, and D. J. Bergman, Phys. Rev. Lett. **87**, 167401 (2001).
[23] S. Zhang, W. Fan, N. C. Panoiu, K. J. Malloy, R. M. Osgood, and S. R. J. Brueck, Phys. Rev. Lett. **95**, 137404 (2005).
[24] G. Dolling, C. Enkrich, M. Wegener, C. M. Soukoulis, and S. Linden, Science **312**, 892 (2006).
[25] *COMSOL Multiphysics User's Guide, Version 3.3* (Comsol AB, Burlington, MA, 2006).
[26] M. A. Ordal, L. L. Long, R. J. Bell, S. E. Bell, R. R. Bell, R. W. Alexander, Jr., and C. A. Ward, Appl. Opt. **22**, 1099 (1983).
[27] D. R. Smith, S. Schultz, P. Markos, and C. M. Soukoulis, Phys. Rev. B **65**, 195104 (2002).
[28] V. Yannopapas, Phys. Rev. B **73**, 113108 (2006).